Thermodynamics of a nonionic sponge phase

T. D. Le,* U. Olsson,[1] H. Wennerström,[1] and P. Schurtenberger[2]
[1]*Center for Chemistry and Chemical Engineering, Phys. Chem. 1, Lund University, P.O. Box 124, S-221 00 Lund, Sweden*
[2]*Institut für Polymere, ETH Zürich, 8092 Zürich, Switzerland*
(Received 17 February 1999)

Different suggestions for the mechanism governing the narrow stability of the L_3 (sponge) phase have led to a series of debates in recent years. There have been several models developed to describe such a mechanism via thermodynamics. To date, experimental data are insufficient to test present theories. In this study, we revisit the sponge phase with two series of thermodynamic data performed on the well-characterized $C_{12}E_5$–*n*-decane–H_2O system. These thermodynamic data sets stem from phase equilibrium and static light scattering experiments designed to link system-specific parameters such as the temperature dependence of the spontaneous curvature H_o and the two bending moduli κ and $\bar{\kappa}$, which have only been loosely connected in earlier experiments. The use of a well-characterized system is important in that it allows usage of molecular descriptors from earlier studies to reduce fit parameters. Another advantage for using this system is that its phase behavior is analogous to a two-component system which, from an experimental standpoint, is more practical to perform accurate measurements and, from a theoretical standpoint, more simple to model. In the present investigation, we use these tools to quantitatively test parameters obtained by different experimental techniques and assumptions inherited in theoretical models designed to interpret them. [S1063-651X(99)02210-2]

PACS number(s): 65.50.+m, 05.70.−a, 64.70.−p, 78.35.+c

I. INTRODUCTION

Since the discovery of an anomalous isotropic liquid phase in the Aerosol OT-water-NaCl system by Fontell some 25 years ago [1], this phase has been found in a great variety of amphiphilic systems [2–5]. Today, it is referred to as the L_3 (or sponge) phase, and its structure has been deduced by small-angle neutron scattering (SANS) [6,7], small-angle x-ray scattering (SAXS) [8,9], light scattering [10,11], conductivity [12,13], self-diffusion NMR [14,15], and visually confirmed by freeze fracture electron microscopy (FFEM) [16] to be a multiply connected bilayer structure that divides a solvent into two interwoven labyrinths. Pictorially, it is envisioned as a spongelike fluid membrane. Its structure resembles the bicontinuous microemulsion (monolayer vs bilayer) and cubic (ordered vs disordered) analogs; and useful structural analogies have been made between them [17–19]. Early studies on the L_3 phase have focused on its unique properties such as the absence of long-range order [20], existence at high dilution [12], Newtonian flow behavior at low shear [21], and streaming birefringence at higher shear rate [22].

Recently, there has been a number of studies exploring possible applications of the sponge phase, such as its use as a model structure for studying intracellular membranes (e.g., endoplasmic reticulum [23], Golgi apparatus, and related microstructures) or as drug transport vehicles [24]. Despite the broad research interests in the L_3 phase, the fundamental thermodynamics that provides insights into its stability is less understood (there is an ongoing debate) and, thus, warrants further investigation.

There have been several models developed to explain the physical phenomena surrounding the L_3 phase [3,4,18,25,26]. The success of these models relies on their ability to provide adequate explanation for the unusually narrow stability range and transitions to neighboring phases. A recent model [27], based on the elastic curvature energy concept, has qualitatively captured these features. It, however, has been under intense debate due to exclusions of some terms and oversimplification of the sampling system, viz, ignoring entropy and Gaussian curvature contributions [28–31]. These issues form the basis of our present investigation.

Taking the latter issue first, we begin our investigation with a well-characterized system that contains three components: a nonionic surfactant ($C_{12}E_5$), an oil (*n*-decane), and a solvent (water) [32]. The additive decane is water insoluble, thus yielding a similar phase behavior (lyotropic phase sequence) as its two-component analog $C_{12}E_5$-H_2O [12] and allowing it to be modeled as a *pseudo*-binary system. A cross section of this system is shown in Fig. 1 where $\Phi=\Phi_s+\Phi_o$ represents the total volume fraction of surfactant and oil at fixed surfactant/oil ratio ($\Phi_s/\Phi_o=0.815$). An equilibrium L_3 phase at various concentrations is highlighted in filled symbols. A common observation in a two-dimensional phase diagram is that the L_3 phase is found to be stable over a broad concentration range (in this case, surfactant and oil), but has a narrow stability range perpendicular to the dilution path (in this case, typically less than 1 °C).

There are some important factors behind our decision for using this three-component system. First, we chose a nonionic system to avoid complications with long-range electrostatic interactions [33]. Secondly, the sponge phase at the selected T-Φ cut occurs at lower temperatures as compared to its binary counterpart, $C_{12}E_5$-H_2O. This is an advantage, but is not our reason for choosing a nonionic system since there are more compacted nonionic surfactants which form L_3 phases at a more suitable experimental temperature range.

*Electronic address: Thao.Le@fkeml.lu.se

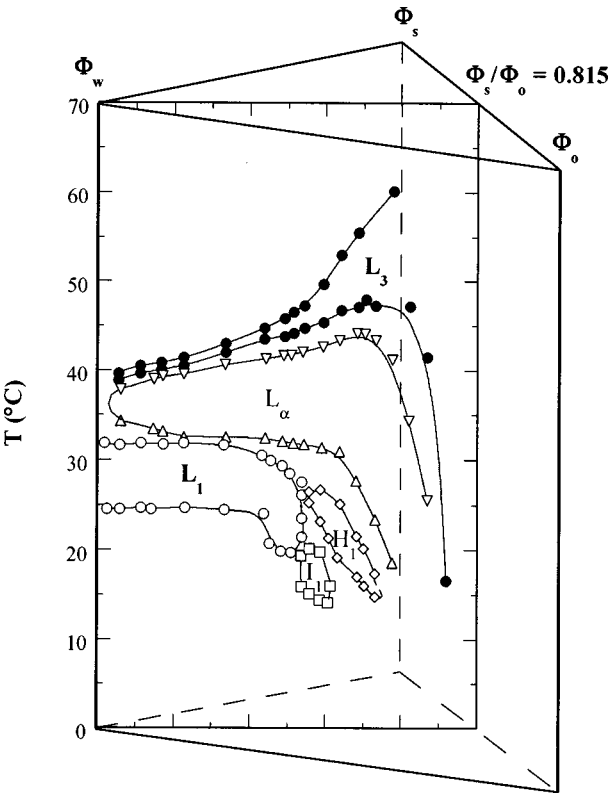

FIG. 1. T-Φ cross section of the $C_{12}E_5$–n-decane–H_2O phase prism (adapted from Ref. [32]). The T-Φ plane is at fixed $C_{12}E_5$–n-decane ratio ($\Phi_s/\Phi_o=0.815$). The phases shown are the L_3 (sponge), L_α (lamellar), L_1 (microemulsion), I_1 (cubic), and H_1 (hexagonal).

Our compromise for a ternary system is that the $C_{12}E_5$ monolayer is simultaneously saturated in both oil and water. This would allow us to use data from the microemulsion to reduce the number of fit parameters. As well, it would allow us to perform a comparative analysis between the L_3 phase and the well-studied droplet microemulsion (L_1) phase occurring at a lower temperature range for the same system (see Fig. 1). It is well accepted that the spontaneous monolayer curvature H_o is strongly temperature dependent for these nonionic surfactants [17,34]. For this ternary system, we can use the microemulsion to better characterize the temperature dependence; while in the binary system, the functional form is more complicated and the temperature at which $H_o=0$ cannot independently be determined [35].

With this system, we performed two series of experiments designed to elicit thermodynamic information on the L_3 phase. The first is a series of phase equilibrium experiments where we carefully examine its uniquely narrow stability limits that extend over a broad concentration range. The second is a series of static light scattering (SLS) experiments where we monitor the scattering intensity as a function of the scattering vector q, temperature, and concentration. These two data sets are designed to link together key system-specific parameters such as H_o, κ, and $\bar{\kappa}$, which we will discuss in detail later. Our objective here is to get all the data on a quantitative level so that we can provide a self-consistent interpretation for these independently determined data sets.

The outline of this paper is as follows. We begin with the Experimental Section which describes the materials and experimental setups. We move next to the Result and Discussion section where we briefly highlight key concepts of the flexible surface approach, and lead from there to the revised form of the free energy which now contains the Gaussian curvature and entropy terms. We then test this revised form by using it to analyze the phase equilibrium and light scattering data. We further test for self-consistency by performing comparative analysis between the L_3 and L_1 phase (formed at lower temperatures). Finally, we close the paper with some concluding remarks.

II. EXPERIMENTAL SECTION

A. Materials

Penta-ethyleneglycol mono n-dodecyl ether ($C_{12}E_5$), with a purity of +99% and a density of 0.9665 g cm^{-3}, was purchased from Nikko Chemicals Co. (Tokyo, Japan). n-Decane, with a purity of +99% and a density of 0.730 g cm^{-3}, was purchased from Sigma Chemicals (Steinheim, Germany). Both substances were used without further purification. Millipore filtered water, with low ion concentration (2 μS cm^{-1}) and a density of 0.998 g cm^{-3}, was used as the diluent.

B. Sample preparation

Samples were prepared by diluting a stock mixture of $C_{12}E_5$–n-decane ($\Phi_s/\Phi_o=0.815$) with Millipore filtered water. The samples were thoroughly mixed in the L_1 and L_3 phases. The sample tubes were then placed, fully submerged, into a thermostatic water bath where we carefully look for the L_3/W and L_3/L_α phase boundaries. Crosspolarizers were used to detect birefringence in the L_3-L_α transition. The bath temperature was raised and lowered in increments of ± 0.05 °C a few times to confirm the phase boundaries.

Samples for the ''fish'' plot were prepared using equal volumes of n-decane and water and varying concentrations of $C_{12}E_5$. The sealed sample tubes were fully submerged in a thermostatic water bath and allowed to equilibrate until phase volumes remained constant over a period of time. As before, the bath temperature was raised and lowered a few times to confirm the phase boundaries.

C. Static light scattering

Static light scattering measurements were performed on a commercial goniometer system (ALV/DLS/SLS-5000F monomode fiber compact goniometer system equipped with an ALV-5000 fast correlator). There have been a number of modifications done on this setup, some of which included a broader temperature range (−6–220 °C) and an improved temperature stability (±0.01 °C for several hours). Two cylindrical scattering cells (8 and 4.2 mm inner diameter) were used to correct for sample transmission and to demonstrate the absence of multiple scattering. Scattering cells were filled with a minimum amount of sample (approximately 10 mm in height) and sealed with a Teflon plug that nearly touched the meniscus of the sample. Such preparation minimizes the temperature gradient in the cell—a necessary procedure to get accurate light scattering measurements on the narrow L_3 phase.

Measurements were performed as a function of scattering angle θ, from $15° \leqslant \theta \leqslant 150°$ in increments of 2°. Ten measurements in intervals of 10 s were averaged for each angle. The data were then corrected for background scattering (cell and solvent) and converted to absolute scattering intensities via $\Delta R(q)$, the ''excess Rayleigh ratio.'' Toluene was used as the reference solvent. The excess Rayleigh ratio was calculated using

$$\Delta R(q) = \frac{\langle \Delta I(q) \rangle}{\langle I_{\mathrm{ref}}(q) \rangle} R_{\mathrm{ref}} \left(\frac{n}{n_{\mathrm{ref}}} \right)^2, \tag{1}$$

where $\langle \Delta I(q) \rangle$ and $\langle I_{\mathrm{ref}}(q) \rangle$ are the averaged excess scattering intensity of the solution and the averaged scattering intensity of the reference solvent, $R_{\mathrm{ref}} = 39.6 \times 10^{-4}\ \mathrm{m}^{-1}$ is the Rayleigh ratio of toluene, $n[= n_w + \Phi(dn/d\Phi)]$ and n_{ref} are the refractive indices of the sample and reference solvent, $dn/d\Phi(=0.11)$ is the refractive index increment, and $q = 4\pi n/\lambda_o \sin(\theta/2)$ is the magnitude of the scattering vector.

This procedure was repeated at other temperatures inside the L_3. For the most part, we initiated measurements at the lower phase boundary and stepped 0.05 °C until the L_3/W coexistence phase boundary was reached. The two-phase boundary was confirmed by visual inspection at the meniscus of the sample and by the distinctively different scattering profiles.

III. RESULTS AND DISCUSSION

A. Free energy model

As outlined above, we have quantitative data from phase equilibrium and from light scattering experiments for the same system measured under compatible experimental conditions. Both data sets are thermodynamic in nature and depend on the free energy of the system. As such, we can interpret these experimental results by formulating a free energy expression containing parameters relating to both data sets. This approach, as we will show, allows the use of molecular descriptors from the oil-in-water droplet microemulsion (L_1 phase, occurring at a slightly lower temperature) to reduce the fit parameters. In principle, this phase can be described within the same model provided that the difference in spontaneous curvature is taken into account.

We begin with a brief overview of the flexible surface model. Its application to surfactant-oil-water systems basically consists of an interfacial description focusing on a curvature free energy density of the polar-apolar interface. To lowest order in curvature, it is commonly written as [36]

$$g_c = 2\kappa(H - H_o)^2 + \bar{\kappa} K, \tag{2}$$

where H and K are the local mean and Gaussian curvatures, respectively. H_o, κ, and $\bar{\kappa}$ are three system-specific parameters: H_o is the spontaneous curvature, $\kappa\ (\geqslant 0)$ is the bending rigidity of the film, and $\bar{\kappa}$ is the so-called saddle splay modulus—the sign and magnitude of which represent the preferred topology of a curved surface. As a sign convention, we adopted the curvature towards oil as positive. For a given film configuration, the *total* curvature free energy G_c is obtained by integrating the curvature free energy density over the interfacial area:

$$G_c = \int g_c dA. \tag{3}$$

In a series of papers [27,37–39], we have argued in favor of a free energy per unit volume for the sponge and balanced microemulsion phases to be of the form

$$G/V = a_3 \Phi^3 + a_5 \Phi^5, \tag{4}$$

where Φ is the volume fraction of the surfactant film. A term linear in Φ is omitted since it can be included in the standard free energy. The leading cubic term emerges from the Porte *et al.* [25] general scaling argument based on the length scale invariance of the curvature energy at $H_o = 0$. In practice, to be able to account for the finite swelling of the sponge and microemulsion phase the a_3 term needs to be negative and a positive higher-order term, which by symmetry is quintic in Φ, is needed to provide stability at higher concentrations. In the microemulsion case, the coefficient a_5 can be obtained by expanding the free energy density to fourth order in curvature. In the bilayer structure of the sponge phase, however, a term quintic in Φ is obtained by evaluating the free energy density, Eq. (2), at the two oppositely oriented monolayers. The use of a monolayer description for bilayer structures, e.g., the sponge phase, might appear unwarranted but has in fact several advantages. An important advantage is being able to use the same formalism for all structures in the surfactant-oil-water phase diagram. This is very useful in that a direct comparison between monolayer and bilayer structures is possible and that the general behavior of H_o becomes much more apparent. A possible weakness in applying Eqs. (2)–(4) to the sponge phase may be that this approach captures only one out of several unknown contributions to the a_5 term. For the present system, these terms appear to be of minor importance, if not negligible.

In a previous paper [40], we have proposed that the important driving mechanism for creating the sponge phase is that its complex topology, characterized by a negative Gaussian curvature, is represented by a negative mean curvature at the polar-apolar interface. As such, the curvature energy is minimized with respect to the mean curvature when the spontaneous curvature H_o is negative. In this description, coefficients a_3 and a_5 are of the forms [27]

$$a_3 = \frac{2\kappa H_o}{l^2} \tag{5a}$$

and

$$a_5 = \frac{\kappa}{2l^3}, \tag{5b}$$

where $2l$ is the bilayer thickness. The terms in Eqs. (5a) and (5b) arise from a bilayer geometry modeled as parallel surfaces. An important property here is that the mean curvature of the monolayers is concentration dependent [40], i.e.,

$$\langle H \rangle \approx -\frac{\Phi^2}{2l}. \tag{6}$$

From this basis, we extend the general form of Eq. (4) to include a Gaussian curvature term and an entropy term. The Gaussian curvature term has a similar scaling as $\langle H \rangle$ and is of the form [40]

$$\langle K \rangle \approx -\frac{\Phi^2}{2l^2}. \tag{7}$$

Its contribution to the a_3 term is [41]

$$a_{3,\mathrm{Gauss}} = -\frac{\overline{\kappa}}{2l^3}. \tag{8}$$

The entropy term is more difficult to determine. We, however, can approximate it using the ideal scaling argument which leads to

$$-\frac{TS}{V} = \frac{A_e}{l^3}\Phi^3, \tag{9}$$

where A_e is expected to have a negative sign such that the entropy density increases with increasing concentration [38,42]. This term is analogous to the undulation contribution to the free energy of a lamellar phase, except for the sign of the numerical coefficient. Parameter A_e depends explicitly on the elastic moduli κ and $\overline{\kappa}$ and is expected to decrease in magnitude when κ increases—again analogous to the lamellar phase.

The addition of the Gaussian curvature and entropy terms to a_3 leads to the free energy density expression of the form [43]

$$G/V = \frac{\kappa}{2l^3}(4lH_o + \alpha)\Phi^3 + \frac{\kappa}{2l^3}\Phi^5, \tag{10}$$

where

$$\alpha = \frac{2A_e - \overline{\kappa}}{\kappa}. \tag{11}$$

B. Temperature dependence of H_o

We have performed experiments over a relatively narrow temperature range between 39 and 43 °C. In these experiments, the system is unusually sensitive to temperature; and this temperature dependence is reflected in the temperature dependence of the free energy. A number of experimental studies [17,34] performed on nonionic systems containing alkylpolyoxyethylene glycol ethers have demonstrated that this temperature dependence is related to changes in the spontaneous curvature H_o. Over a small temperature range, kT varies marginally and, thus, the temperature dependence in the first order of the elastic moduli can be neglected. A Taylor expansion about the phase-inversion temperature (PIT) yields

$$H_o(T) \cong \left.\frac{dH_o}{dT}\right|_{T_o}(T_o - T) + \cdots \approx \beta(T_o - T), \tag{12}$$

where β is a temperature coefficient and T_o is the temperature at the balanced point where $H_o = 0$. Phase equilibrium and direct radius measurements of microemulsion droplets indicate that this linear term adequately accounts for the temperature dependence of H_o—covering as large of a temperature range as ± 20 °C around the PIT.

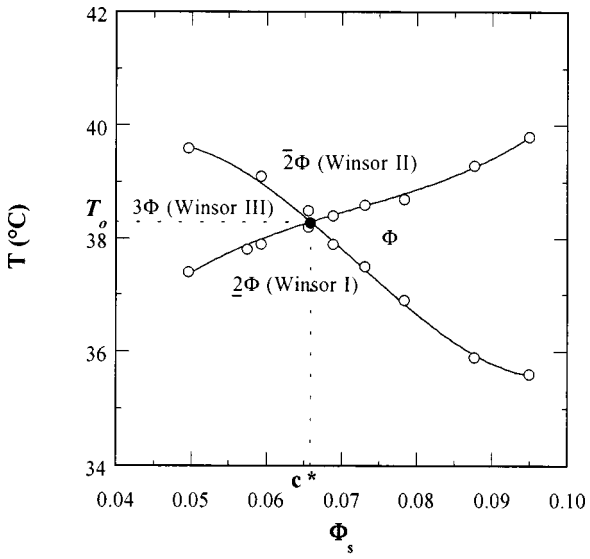

FIG. 2. Kahlweit plot illustrating an independent measurement of the temperature T_o where $H_o = 0$. T_o is found to be 38.3 °C at the phase-inversion temperature (PIT) marked by a filled symbol. A lamellar phase commonly found at higher surfactant concentration is not shown since it is outside the scope of this study.

With Eqs. (10)–(12), we can now group the phase equilibrium and light scattering results for a unified interpretation. There are four undetermined parameters (α, β, κ, and T_o) in these equations, all can be accessible by experiments.

C. T_0 determined at the phase-inversion temperature

The value of T_o at which $H_0 = 0$ was independently determined from a Kahlweit- (''fish'') plot [44], where the phase equilibria of the same system containing equal volumes of oil and water was monitored as a function of temperature and surfactant concentration. The experimental data are shown in Fig. 2. Within the flexible surface model, the microemulsion phase containing equivolumes of oil and water has its maximum swelling at $H_o = 0$. For the present system, this occurs at $T_o = 38.3$ °C.

D. Membrane characteristic length and volume fraction

For curved monolayers, it is important to specify the interface where area and curvature are evaluated. Studies on nonionic systems have demonstrated that the polar-apolar interface separating the alkyl and penta ethylene oxide blocks of $C_{12}E_5$ is neutral, i.e., its area does not depend on the curvature. Based on these findings, we define the effective membrane (bilayer) volume fraction for the present system as

$$\Phi_m \cong 0.5\Phi_s + \Phi_o = 0.775\Phi, \tag{13}$$

where $\Phi(=\Phi_s + \Phi_o)$ and the subscripts denote the volume fractions of surfactant and oil, respectively. The term $0.5\Phi_s$ arises from the fact that the alkyl chain volume corresponds to about half of the total molecular volume of the $C_{12}E_5$

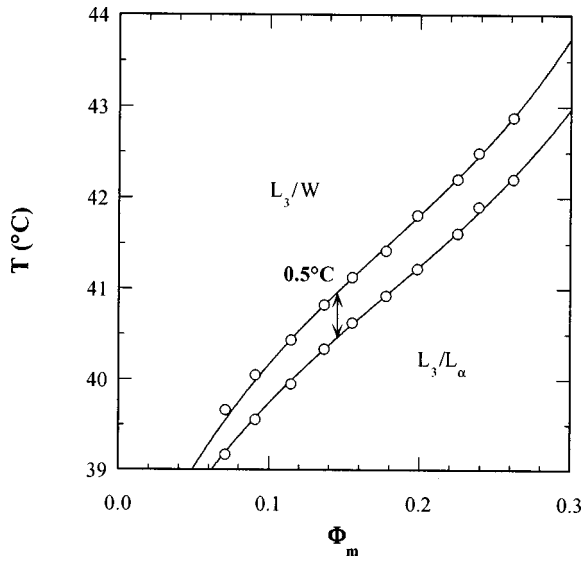

FIG. 3. The L_3 phase investigated in this study is stable within a narrow temperature range. Beyond this stability range, the sponge phase coexists with a dilute solution at higher temperature, and lamellar phase at lower temperature. The membrane volume fraction Φ_m is based on the description presented in Sec. III D.

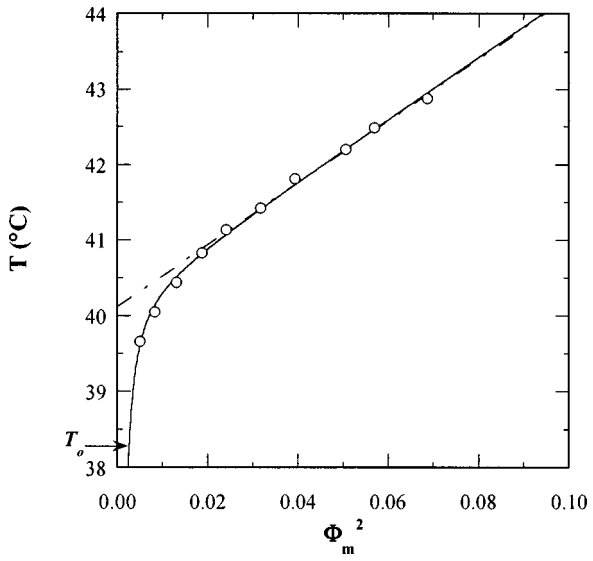

FIG. 4. Plot of T vs Φ_m^2. Experimental L_3/W coexistence boundaries are represented by open symbols. The best fit using Eq. (15) yields $\alpha=8.90\times10^{-2}$ and $\beta=4.88\times10^6\,\mathrm{K}^{-1}\,\mathrm{m}^{-1}$ (dashed line), and the best fit using Eq. (17) yields $\Pi_W=2.06\times10^{-9}kT$ (solid line).

molecule. For the present system, the Φ_m in Eq. (13) is the volume fraction that enters the free energy density expression. The volume of a $C_{12}E_5$ molecule is approximately 700 Å^3, and the area it occupies at a defined polar-apolar interface in the $C_{12}E_5$–n-decane–H_2O system is 48 Å^2. For the present surfactant/oil ratio, this results in a bilayer thickness of 50 Å; hence the value of l that enters the free energy density is 25 Å.

E. Thermodynamic data from phase equilibrium experiments

L_3 phases are generally narrow as compared to other phases (Fig. 1). This is particularly true in our cut of the $C_{12}E_5$–n-decane–H_2O phase prism, where the L_3 has a width of approximately 0.5 °C (Fig. 3). Such narrow stability requires careful and accurate determination of the equilibrium phase boundaries such that the data collection in SLS experiments could be optimized to yield a more accurate value of κ, i.e., through fits to a model. Another matter of importance is to keep the membrane composition constant for all experiments. This was done by preparing a stock solution containing a fixed ratio of $C_{12}E_5$/decane and diluting it with water to get different compositions. These procedures are necessary for minimizing experimental errors so that the data from different experiments could be compared on a quantitative level and for checking consistency in their interpretation.

As shown in Fig. 3, the upper temperature limit of the L_3 phase is marked by a phase separation with predominately pure water. Equilibrium with pure water implies that the water chemical potential of the sponge phase is equivalent to that of the reference state (pure water). In other words, the osmotic pressure $\Pi=\Delta\mu_w/\nu_w$ is zero. This is related to the free energy as

$$\Pi=\Phi\frac{\partial}{\partial\Phi}(G/V)-G/V, \tag{14}$$

and solving Eq. (14) for $\Pi=0$ gives $T_{L_3/W}$ as a function of the bilayer volume fraction:

$$T_{L_3/W}=\frac{\Phi_m^2}{2l\beta}+\frac{\alpha}{4l\beta}+T_o. \tag{15}$$

Equation (15) explicitly shows that a plot of T_{L_3} versus Φ_m^2 is expected to yield a straight line and that parameters α and β can be obtained from a least-squares fit. Figure 4 illustrates such a plot, and linearity (dashed line) is found over a substantial concentration range. The best fit yields $\alpha=0.089$ and $\beta=4.88\times10^6\,\mathrm{K}^{-1}\,\mathrm{m}^{-1}$.

It is clear that there are deviations from linearity at lower concentrations. This nonlinear behavior can be attributed to the finite monomer solubility that prevents the L_3 phase from swelling infinitely. If the surfactant monomer concentration in the excess water phase W is slightly higher than in the L_3 phase, this results in an osmotic stress on the L_3 and pushes the phase boundary to a higher concentration. If we consider a constant excess monomer pressure in the water phase, Π_W, we can solve for a more general case using

$$\Pi=2a_3\Phi_m^3+4a_5\Phi_m^5=\Pi_W, \tag{16}$$

from which the phase boundary temperature is given by

$$T_{L_3/W}=\frac{2\Phi_m^2+\alpha}{4l\beta}-\Pi_W\left(\frac{l^2}{4\kappa\beta\Phi_m^3}\right)+T_o. \tag{17}$$

Substituting into Eq. (17) the values for α and β from above and $\kappa=2.5kT$ from static light scattering measurements (discussed below) leaves Π_W as a single fit parameter. The best fit (solid line in Fig. 4) yields $\Pi_W\approx2.06\times10^{-9}\ kT\,\mathrm{m}^{-3}$. This value is small; and if we treat it as surfactant monomers in an ideal solution, i.e., $\Pi_W=c_skT$, we find that it corresponds to a surfactant concentration c_s

$=2\times10^{-6}M$, which is an order of magnitude smaller than the critical micellization concentration (CMC) of the surfactant, $6\times10^{-5}M$. Thus, by factoring in the finite pressure in the water phase we can account for the phase boundary over the entire concentration range. The actual value of Π_W is not so important here since it is very small and that a small amount of impurity can induce such an effect. What is important is that the overall result is clear: At low concentrations, the osmotic compressibility becomes very high such that the phase boundary becomes sensitive to minor perturbations. This effect is expected to be dominated by the surfactant solubility since it is close to two orders of magnitude higher than the oil solubility in water.

F. Thermodynamic data from static light scattering experiments

Static light scattering experiments were performed on five different concentrations ranging from $\Phi_m=0.071$ to $\Phi_m=0.262$. For each concentration, measurements were made at four to six different temperatures inside the L_3 phase. Figures 5(a) and 5(b) are two representative plots of $1/\Delta R(q)$ versus q^2 for the most diluted and concentrated samples, respectively. The data were fitted with the Ornstein-Zernike form based on the Lorentzian scattering law

$$\frac{1}{\Delta R(q)}=\frac{1}{\Delta R(0)}(1+q^2\xi_s^2), \tag{18}$$

where $\Delta R(0)$ is the excess Rayleigh ratio at zero wave vector ($q=0$), and ξ_s is the static correlation length. For dilute samples, linear fits were made using only data in the Guinier (low q) limit, see Fig. 5(a). For concentrated samples, fits were made using data in the full q range, see Fig. 5(b). Extrapolated values of $\Delta R(0)$ are presented as a function of the temperature in Fig. 6. An important feature here is the strong temperature dependence of scattered intensity.

There is a direct relationship between $\Delta R(0)$ and the free energy density [Eq. (10)] i.e.,

$$\Delta R(0)=\chi kT\left[\frac{\partial^2(G/V)}{\partial\Phi_m^2}\right]^{-1}, \tag{19a}$$

with

$$\chi=\frac{4\pi^2n_w^2}{\lambda_o^4}\left(\frac{dn}{d\Phi_m}\right)^2, \tag{19b}$$

where n_w is the refractive index of water, $dn/d\Phi_m$ is the refractive index increment, and λ_o is the wavelength of the incident light in vacuum. A value for $dn/d\Phi(=0.11)$ has been determined previously at 25 °C [45] and is not expected to vary significantly with temperature. We can use this value as follows: $dn/d\Phi_m=(0.775)^{-1}(dn/d\Phi)$. From Eqs. (10)–(13), (19a), and (19b), we get the forward scattering intensity as a function of temperature:

$$\Delta R_o(T)=\frac{kT}{\kappa}\left[\frac{\chi l^3}{3\Phi_m\alpha+12\Phi_m l\beta(T_o-T)+10\Phi_m^3}\right]. \tag{20}$$

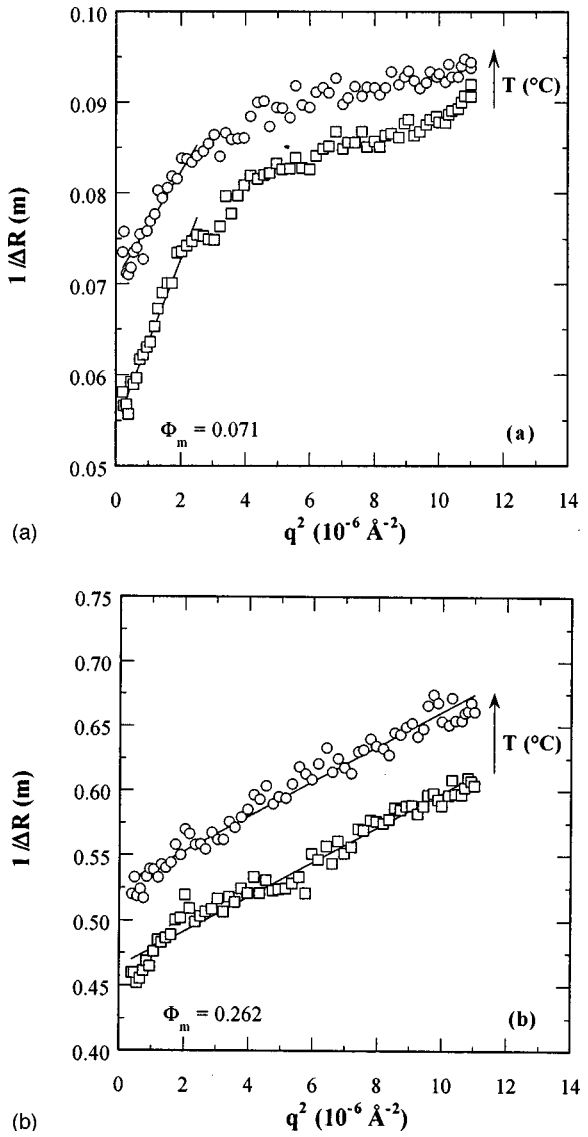

FIG. 5. Static light scattering spectra plotted as $1/\Delta R$ vs q^2. (a) For dilute samples, fits using Eq. (18) were made in the low-q limit. (b) For concentrated samples, linear fits were made over the entire q range.

From SLS experiments, we obtained 25 independent measurements of the scattering intensity.

Instead of making a global three-parameter fit, we choose to implement our predetermined parameters α and β from the phase equilibrium experiments, which leaves κ as the *only* adjustable parameter. For five different concentrations, the best fits using Eq. (20) yield a value of $\kappa=2.5kT$ (solid lines in Fig. 6). An important feature here is that this single fit parameter describes both the concentration and temperature dependence of the forward light scattering data. These are nontrivial properties of the free energy expression, Eq. (10), and provide strong support for this approach. Earlier light scattering measurements on L_3 phases were complicated with large errors contributed by less precise experimental conditions and, therefore, cannot be used to test free energy expressions. In the present study, this matter has been resolved as evidenced by the quantitative agreement between parameters from phase equilibrium and light scattering experiments.

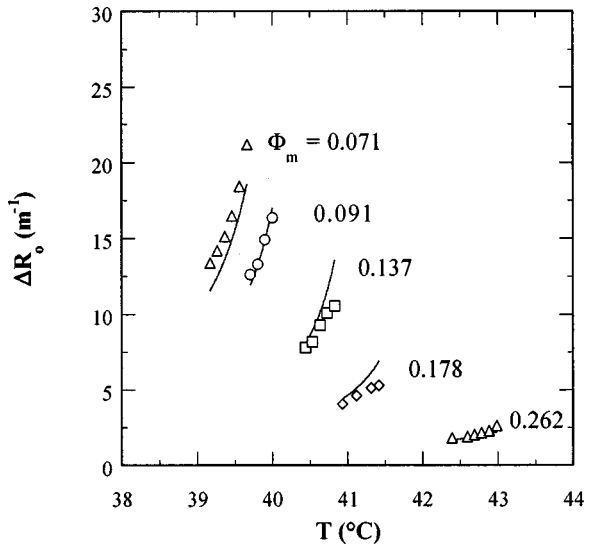

FIG. 6. Temperature dependence of the Rayleigh ratio at zero scattering vector ($q=0$). Shown are experimental data points (symbols) and theoretical calculations (solid lines). These calculations are based on Eq. (20) where fits were individually performed for each concentration. The bending modulus κ was determined from best-fit results to be $2.5kT$ ($\pm 10\%$); and this value was used to get the calculated curves.

The results up to now indicate that the free energy of Eq. (10) coupled with the well-accepted linear temperature dependence of H_o [Eq. (12)] successfully and self-consistently describes both the phase equilibrium with excess solvent and the forward light scattering of the L_3 phase. In the analysis of these experiments, we obtained values for α, β, and κ, the former of which contains both the Gaussian curvature and entropy terms and was found to be small. This small value can be considered as a minor offset of the spontaneous curvature. The omission of α in previous studies [27,39] is, therefore, not a serious error.

We can now proceed and compare these results with previously published data on the droplet microemulsion (L_1) phase of the same system occurring at lower temperature. Such a comparison would provide additional means to test the free energy and a complementary set of thermodynamic data to determine the contributions of $\bar{\kappa}$ and A_e to the parameter α. Before proceeding with that, we need to analyze the uncertainties in the obtained parameters. This is important when comparing between different experiments.

G. Uncertainties in experimental methods

By combining the phase equilibrium and light scattering results, we have arrived at a set of fitted parameters that enter the free energy expression. The accuracy of these parameters depends both on experimental uncertainties and on assumptions inherent in Eq. (10). The fact that we get a consistent interpretation of the experimental data using Eq. (10) strongly indicates that the functional form is correct. There remain, however, uncertainties in coefficients a_3 and a_5 which may introduce another uncertainty in the evaluated parameter values; these are needed for a quantitative interpretation.

From the part of the curve in Fig. 4 which yields a straight line, we can determine the slope with a relative accuracy better than 5%. In the free energy expression, this slope is exclusively attributed to the temperature dependence of the spontaneous curvature through the coefficient β. This is certainly the dominant contribution, but in arriving at Eq. (15) we have made a number of assumptions which may introduce some systematic errors in β. We have little *a priori* knowledge concerning contributions of the temperature dependence to a_3 and a_5 except for the fact that the effects of H_o dominate. However, if we make a simple assumption that these contributions are proportional to T, as is the entropy contribution, then we expect a 1% change over a 3° change. Factoring this error into both a_3 and a_5, we get a correction of less than 5%. There is also an experimental uncertainty in the monolayer thickness $l=(25\pm 2)$ Å, which is also a part of the slope and needs to be considered. This error introduces another 8% uncertainty in β. From this, we conclude that $\beta(=4.88\times 10^6\,\mathrm{K^{-1}\,m^{-1}})$ is reasonably accurate in that the combined uncertainty is within $\pm 15\%$.

From the phase equilibrium data, we can also determine the contribution of α to the coefficient a_3. In Fig. 4, The primary fit parameter is the intercept of the straight line where the numerical accuracy is within ± 0.2 °C. To obtain α, we use the balanced temperature T_o from the microemulsion that was measured with an accuracy of ± 0.1 °C. There is an assumption involved in treating H_o as a field variable; that is, H_o is dependent only on temperature and not on composition. Considering the amounts of oil and water present, the $C_{12}E_6$ monolayer is equally saturated with solvents in the L_3 phase as it is in the balanced microemulsion. The temperature T_o determined in the balanced microemulsion is, therefore, not expected to differ significantly from T_o at the lower surfactant/oil ratio that we have in the L_3 phase. Hence, we only expect a random uncertainty in the fitted parameter $\alpha(=0.089)$ to be within $\pm 15\%$.

The bending rigidity κ was determined from the light scattering data to be $2.5kT$, corresponding to 1.1×10^{-20} J for a mean temperature in the experimental range 39–43 °C. The uncertainty in the fits is within $\pm 10\%$. The parameters α and β that enter into the expression for $\Delta R(0)$ were determined from the slope in Figs. 5(a) and 5(b) and do not give rise to any substantial uncertainty in κ. However, $\Delta R(0)$ is proportional to the third power of l which carries a 10% uncertainty and, thus, introduces a 30% uncertainty in κ. Additionally, there is a systematic uncertainty due to the choice of the a_5 coefficient which can be obtained from a more abstract analysis using the light scattering data. Other contributions to a_5 are expected to be positive such that the value for κ is smaller. At the present time, we do not have an accurate estimate for the magnitude of this correction which would lead to a more precise interpretation of α.

H. Comparative analysis with the droplet microemulsion phase

As shown in Fig. 1, this system has a microemulsion phase (L_1) in the temperature range between 25 °C and 32 °C where the structure is sensitive to temperature, i.e., the mean curvature is decreasing with increasing temperature. In the vicinity of the lower phase boundary the structure is that of spherical oil droplets with an average radius of 75 Å [46], a value measured at the neutral surface (enclosing oil and the

surfactant alkyl chains, see above). The spherical shape corresponds to the maximum curvature towards oil constrained by a constant area-to-enclosed volume ratio, i.e., at fixed Φ_s/Φ_o ratio. Below the temperature of 25 °C, the spontaneous curvature is increased and phase separation occurs as the result of spherical droplets decreasing their radius and expelling oil to the excess phase. This scenario was analyzed by Safran and co-workers and has since been referred to as the emulsification failure [47]. We can draw an analogy between the droplet/oil coexistence and the L_3/W coexistence since both regulate the monolayer curvature through the solvent concentration.

The free energy for a dispersion of spherical droplets can be written as

$$G/V = G_c/V + G_{\mathrm{mix}}/V, \tag{21}$$

where G_c is the curvature energy part and G_{mix} is the mixing or translational entropy. The curvature energy part is of the form

$$G_c/V = \frac{4\pi\Phi}{\nu_{\mathrm{mic}}}[2\kappa(1-RH_{\mathrm{o}})^2+\bar{\kappa}]. \tag{22}$$

The droplets interact as hard spheres [48], and from the Carnahan-Starling equation of state we have

$$G_{\mathrm{mix}}/V = \frac{\Phi kT}{\nu_{\mathrm{mic}}}\left[\ln\left(\Phi\frac{\nu_w}{\nu_{\mathrm{mic}}}\right)-1+\frac{4\Phi-3\Phi^2}{(1-\Phi)^2}\right], \tag{23}$$

which reduces to ideal mixing at lower Φ. Here, ν_w and ν_{mic} are the water and micellar volumes with the latter given by $\nu_{\mathrm{mic}}=4\pi R^3/3$. For simplicity reasons, we have ignored minor contributions from size and shape polydispersities. This monodispersity approximation is analogous to the approximation in the L_3 phase analysis where the curvature properties are based on the assumption that the midplane of the bilayer lies on a minimal surface of zero mean curvature everywhere.

For the L_3 phase, the upper phase boundary is characterized by the zero water chemical potential. Analogously, the lower phase boundary of the microemulsion phase is characterized by zero oil chemical potential. Solving Eqs. (21)–(23) for $\mu_o=0$ gives a relation between the sphere radius and the spontaneous curvature at the emulsification failure boundary as

$$RH_{\mathrm{o}} = 1+\frac{\bar{\kappa}}{2\kappa}+\frac{kT}{16\pi\kappa}\left[2\ln\left(\Phi\frac{\nu_w}{\nu_{\mathrm{mic}}}\right)+\frac{5\Phi-\Phi^2}{1-\Phi}\right]. \tag{24}$$

The temperature of the lower phase boundary of the L_3 phase has a very weak concentration dependence in the concentration range $0.01<\Phi<0.4$ arising from the fact that the entropic contribution to RH_{o} is dominated by the slowly varying ideal mixing part $\ln\Phi$. Numerical calculations show a significant concentration dependence only for $\Phi<0.01$ and that in the range $0.01<\Phi<0.4$ the entropic contribution is essentially a constant offset, which is approximately $-0.5kT/\kappa$. Since the sphere radius is known, we can calculate H_{o} at 25 °C using the β value obtained in the analysis of the L_3 phase boundary. Doing so, we obtain $H_{\mathrm{o}}^{-1}=154$ Å, a value that is approximately two times the sphere radius, and an approximate relation $\kappa+\bar{\kappa}\approx kT$. Substituting in $\kappa=2.5kT$, we obtain $\bar{\kappa}=-1.5kT$.

Consistency between the descriptions of the L_3 phase and the microemulsion droplet phase can further be tested. In an earlier study, Rajagopalan *et al.* [49] have analyzed the influence of charged droplets on the phase equilibria where it was found that $\kappa\beta=(4\pm0.5)\times10^{-14}\,\mathrm{J\,K^{-1}\,m^{-1}}$ and $2\kappa+\bar{\kappa}=(1.2\pm0.4)\times10^{-20}$ J, corresponding to 2.8 kT at 314 K. The value for the product $\kappa\beta$ obtained from the present analysis of the L_3 phase is slightly larger, $(5.0\pm0.6)\times10^{-14}\ \mathrm{J\,K^{-1}\,m^{-1}}$, but is in reasonable agreement considering the error involved. The value of $2\kappa+\bar{\kappa}$ gives us another opportunity to estimate $\bar{\kappa}$, i.e., subtracting $2\kappa=5.0kT$ gives $\bar{\kappa}=-2.2kT$.

There is another experiment which contains information on the elastic moduli. Sottmann and Strey [50] have recently measured the interfacial tension γ between the droplet microemulsion phase and the excess oil phase for a large number of systems including the present one. The lowest temperature investigated was 28 °C, but can be extrapolated to 25 °C. Doing so, we obtain $\gamma=2\times10^{-4}\,\mathrm{N\,m^{-1}}$. The simplest quantitative interpretation of this interfacial tension involves a transformation from the spherical droplets of radius R to the flat interface between the microemulsion and the oil phase. Taking into account only the curvature free energy [34],

$$\gamma = \frac{2\kappa+\bar{\kappa}}{R^2}, \tag{25}$$

and inserting the values for γ and R yields $2\kappa+\bar{\kappa}=2.7kT$, which agrees well with the value obtained from the study of charged spheres. The curvature free energy is clearly the dominant contribution to the interfacial tension, but is not the only one since including the entropy of mixing in the analysis would lead to a slightly higher value of $2\kappa+\bar{\kappa}$. Our analysis shows that the two values of $2\kappa+\bar{\kappa}$, obtained from two very different experiments, are in agreement with one another.

I. Final estimates of phenomenological parameters

By combining the present experimental results with previous investigations, we have arrived at estimates for the constants β, κ, and $\bar{\kappa}$. All these estimates contain errors contributed by experimental uncertainties and systematic errors introduced by simplifying assumptions in theoretical models which relate, on a quantitative level, to the experimental data and constants yet to be determined.

Fortunately, a coherent picture emerges when combining the different approaches. From all the data that we could gather for this system, we can summarize by providing objectively best estimates for

$$\beta = 5\times10^{6}\,\mathrm{K^{-1}\,m^{-1}}, \tag{26a}$$

$$\kappa = 1\times10^{-20}\ \mathrm{J}\quad (2.5kT\ \text{at}\ 298\ \mathrm{K}), \tag{26b}$$

$$\bar{\kappa} = -8\times10^{-21}\ \mathrm{J}\quad (-2kT\ \text{at}\ 298\ \mathrm{K}), \tag{26c}$$

where the top two are reasonably accurate ($\pm 20\%$) while the uncertainty in $\bar{\kappa}$ is larger ($\pm 2\times 10^{-21}$ J).

From the value of $\bar{\kappa}$, we can also estimate the entropic contribution A_e to the a_3 term of the free energy density. This carries a large uncertainty over to A_e. The parameter $\alpha=(2A_e-\bar{\kappa})/\kappa$ was determined to be 0.089. This small value implies that A_e and $\bar{\kappa}$ are similar in magnitude, but with $\bar{\kappa}<2A_e$ since α is positive. If we use the values $\kappa=2.5kT$ and $\bar{\kappa}=-2kT$, we obtain an estimate for $A_e=-0.9kT$. This could be compared with the value $-0.03kT$ obtained from a random mixing of lattice sites of size d, where $d\approx 3l/\Phi$ is the characteristic pore size of the membrane structure [42]. The difference, although being an order of magnitude, can almost be accounted for by the experimental uncertainty. A more systematic study extending to other systems is needed to better understand the entropy term A_e.

IV. CONCLUDING REMARKS

The thermodynamics of a nonionic L_3 phase has been analyzed using the flexible surface concept. This L_3 phase contains three components, but can be modeled as a *pseudo*-binary system since the additive *n*-decane is insoluble in water, i.e., the solvent is a single component and the bilayer contains only water insoluble components. As demonstrated, this plays an important role in the analysis of the phase equilibrium and static light scattering experiments using the free energy density of the form shown in Eq. (10).

The present system also contains a droplet oil-in-water microemulsion (L_1) phase at a lower temperature range where the spontaneous curvature is positive and where there have been a number of independent investigations. Our analysis using the emulsification failure and interfacial tension data gave complementary information on the curvature elasticity of the surfactant monolayer. A comparison between the properties of the L_1 and L_3 phases provided a self-consistent test of the applied model, and it was found that these phases can be described with the same set of parameters.

While there is a general agreement on the description of the droplet microemulsion in terms of Eqs. (21)–(23), there has been a debate on the thermodynamics of the topologically more complex L_3 phase (and the analogous balanced microemulsion). This debate has drawn considerable attention to the first correction term of the Φ^3 scaling and to the sign of the prefactor. We have argued that the ideal scaling term a_3 is negative and that the first correction term is proportional to Φ^5 with a positive prefactor, see Eq. (4). Other investigators [26,51] have suggested that the a_3 is positive and have included a logarithmic concentration dependence term, i.e.,

$$G/V=(a_3+b_3\ln\Phi)\Phi^3+\cdots, \tag{27}$$

to ensure a finite swelling and equilibrium with excess solvent ($a_3, b_3>0$). Equations (4) and (27) arise from different points of view. Equation (27) reflects the view that stability is governed by fluctuations; and the logarithmic correction term was originally introduced through a renormalization of the elastic constants. Equation (4), on the other hand, is based on the view that the important parameter is the monolayer spontaneous curvature. We, unfortunately, cannot test the renormalization model [Eq. (27)] against our experimental data. Such a test would require specific temperature dependence of the coefficients, which is lacking in Eq. (27).

Instead, we focused our attention on Eq. (4) and searched for an internal consistency in the analysis of the phase equilibria and light scattering data. Such a consistency was found not only limited to the L_3 phase, but on a more global level since the analyses included also the droplet and balanced bicontinuous microemulsions.

ACKNOWLEDGMENT

This research was supported by the Swedish Natural Science Foundation (NFR).

[1] K. Fontell, in *Colloidal Dispersions and Micellar Behavior*, edited by K. L. Mittal, ACS Symposium Series Vol. 9 (American Chemical Society, Washington, D.C., 1974), p. 270.

[2] D. J. Mitchell, G. J. T. Tiddy, L. Waring, T. Bostock, and M. P. McDonald, J. Chem. Soc., Faraday Trans. 1 **79**, 975 (1983).

[3] G. Gompper and M. Schick, *Self-Assembling Amphiphilic Systems* (Academic, San Diego, 1994).

[4] S. A. Safran, *Statistical Thermodynamics of Surfaces, Interfaces, and Membranes* (Addison-Wesley, Reading, MA, 1994).

[5] A.-M. Bellocq, *Flexible Surfactant Films: Phase Behavior, Structure, and Applications* (Dekker, New York, 1996).

[6] D. Gazeau, A. M. Bellocq, D. Roux, and T. Zemb, Europhys. Lett. **9**, 447 (1989).

[7] R. Strey, J. Winkler, and L. Magid, J. Phys. Chem. **95**, 7502 (1991).

[8] A. Maldonado, W. Urbach, R. Ober, and D. Langevin, Phys. Rev. E **54**, 1774 (1996).

[9] N. Lei, C. R. Safinya, D. Roux, and K. S. Liang, Phys. Rev. E **56**, 608 (1997).

[10] D. Roux, M. E. Cates, U. Olsson, R. C. Ball, F. Nallet, and A. M. Bellocq, Europhys. Lett. **11**, 229 (1990).

[11] M. Skouri, J. Marignan, J. Appell, and G. Porte, J. Phys. II **1**, 1121 (1991).

[12] R. Strey, R. Schomäcker, D. Roux, F. Nallet, and U. Olsson, J. Comput. Phys. **86**, 2253 (1990).

[13] C. Vinches, C. Coulon, and D. Roux, J. Phys. II **4**, 1165 (1994).

[14] B. Balinov, U. Olsson, and O. Söderman, J. Phys. Chem. **95**, 5931 (1991).

[15] K. Fukuda, U. Olsson, and U. Würz, Langmuir **10**, 3222 (1994).

[16] R. Strey, W. Jahn, G. Porte, and P. Bassereau, Langmuir **6**, 1635 (1990).

[17] U. Olsson and H. Wennerström, Adv. Colloid Interface Sci. **49**, 113 (1994).

[18] H. Wennerström, J. Daicic, U. Olsson, G. Jerke, and P. Schurtenberger, J. Mol. Liq. **72**, 15 (1997).

[19] S. Hyde, S. Andersson, K. Larsson, Z. Blum, T. Landh, S. Lidin, and B. W. Ninham, *The Language of Shape (The Role*

of Curvature in Condensed Matter: Physics, Chemistry and Biology) (Elsevier, Amsterdam, 1997).
[20] D. A. Antelmi, P. Kékicheff, and P. Richetti, J. Phys. II **5**, 103 (1995).
[21] P. Snabre and G. Porte, Europhys. Lett. **13**, 641 (1990).
[22] H. Pleiner and H. R. Brand, Europhys. Lett. **15**, 393 (1991).
[23] G. Lindblom and L. Rilfors, Biochim. Biophys. Acta **988**, 221 (1988).
[24] K. Alfons and S. Engstrom, J. Pharm. Sci. **87**, 1527 (1998).
[25] G. Porte, M. Delsanti, I. Billard, M. Skouri, J. Appell, J. Marignan, and F. Debeauvais, J. Phys. II **1**, 1101 (1991).
[26] M. E. Cates, D. Roux, D. Andelman, S. T. Milner, and S. A. Safran, Europhys. Lett. **5**, 733 (1988).
[27] J. Daicic, U. Olsson, H. Wennerström, G. Jerke, and P. Schurtenberger, J. Phys. II **5**, 199 (1995).
[28] D. Roux, F. Nallet, C. Coulon, and M. E. Cates, J. Phys. II **6**, 91 (1996).
[29] J. Daicic, U. Olsson, H. Wennerström, G. Jerke, and P. Schurtenberger, J. Phys. II **6**, 95 (1996).
[30] G. Porte, J. Appell, and J. Marignan, Phys. Rev. E **56**, 1276 (1997).
[31] J. Daicic, U. Olsson, H. Wennerström, G. Jerke, and P. Schurtenberger, Phys. Rev. E **56**, 1278 (1997).
[32] M. S. Leaver, U. Olsson, H. Wennerström, R. Strey, and U. Würz, J. Chem. Soc., Faraday Trans. **91**, 4269 (1995).
[33] I. Carlsson and H. Wennerström, Langmuir **15**, 1966 (1999).
[34] R. Strey, Colloid Polym. Sci. **272**, 1005 (1994).
[35] T. D. Le, U. Olsson, H. Wennerström, and P. Schurtenberger, (unpublished).
[36] W. Helfrich, Z. Naturforsch. C **28**, 693 (1973).
[37] H. Wennerström and U. Olsson, Langmuir **9**, 365 (1993).
[38] J. Daicic, U. Olsson, and H. Wennerström, Langmuir **11**, 2451 (1995).
[39] J. Daicic, U. Olsson, H. Wennerström, G. Jerke, and P. Schurtenberger, Phys. Rev. E **52**, 3266 (1995).
[40] D. Anderson, H. Wennerström, and U. Olsson, J. Phys. Chem. **93**, 4243 (1989).
[41] T. D. Le, U. Olsson, and H. Wennerström (unpublished).
[42] D. Andelman, M. E. Cates, D. Roux, and S. A. Safran, J. Chem. Phys. **87**, 7229 (1987).
[43] We remain in the harmonic approximation for the monolayer, which appears to be sufficient. Our Φ^5 term results from the particular concentration dependence of $\langle H \rangle$ [Eq. (6)] for the multiply connected bilayer structure.
[44] M. Kahlweit, R. Strey, and G. Busse, J. Phys. Chem. **94**, 3881 (1990).
[45] U. Olsson and P. Schurtenberger, Langmuir **9**, 3389 (1993).
[46] H. Bagger-Jörgensen, U. Olsson, and K. Mortensen, Langmuir **13**, 1413 (1997).
[47] L. A. Turkevich, S. A. Safran, and P. A. Pincus, in *Surfactants in Solution*, edited by K. L. Mittal and P. Bothorel (Plenum, New York, 1986), Vol. 6, p. 1177.
[48] U. Olsson, H. Bagger-Jörgensen, M. Leaver, J. Morris, K. Mortensen, R. Strey, P. Schurtenberger, and H. Wennerström, Prog. Colloid Polym. Sci. **106**, 6 (1997).
[49] V. Rajagopalan, H. Bagger-Jörgensen, K. Fukuda, U. Olsson, and B. Jönsson, Langmuir **12**, 2939 (1996).
[50] T. Sottmann and R. Strey, J. Chem. Phys. **106**, 8606 (1997).
[51] G. Porte, J. Appell, P. Bassereau, and J. Marignan, J. Phys. (France) **50**, 1335 (1989).